Anomalous dispersion of the acoustic mode in liquid Bi

M. Inui,[1,*] Y. Kajihara,[1] S. Munejiri,[1] S. Hosokawa,[2] A. Chiba,[3] K. Ohara,[4] S. Tsutsui,[4] and A. Q. R. Baron[4,5]

[1]*Graduate School of Integrated Arts and Sciences, Hiroshima University, Higashi-Hiroshima, Hiroshima 739-8521, Japan*

[2]*Department of Physics, Graduate School of Science and Technology, Kumamoto University, Kumamoto 860-8555, Japan*

[3]*Department of Physics, Keio University, Yokohama 223-8522, Japan*

[4]*Japan Synchrotron Radiation Research Institute, SPring-8, Sayo-gun, Hyogo 679-5198, Japan*

[5]*Materials Dynamics Laboratory, RIKEN SPring-8 Center, Sayo-gun, Hyogo 679-5148, Japan*

(Received 14 September 2014; revised manuscript received 5 June 2015; published 25 August 2015)

Inelastic x-ray scattering measurements on liquid Bi were carried out. Prominent acoustic mode excitations were observed in the dynamic structure factor to beyond 12 nm^{-1}, which resolves previously conflicting results as to their presence beyond 6 nm^{-1}. We find the dispersion curve of the excitation energy with momentum transfer is nearly flat from 7 to 15 nm^{-1} consistent with *ab initio* calculations of liquid Bi [J. Souto *et al.*, Phys. Rev. B **81**, 134201 (2010)]. Our *ab initio* and classical molecular dynamics simulations suggest that a long-range force is needed to reproduce the flatness of the dispersion curve, and the long-range force is correlated with a local structure consisting of shorter and longer bonds in the liquid.

DOI: 10.1103/PhysRevB.92.054206 PACS number(s): 61.25.Mv, 61.20.Lc, 47.35.Rs

I. INTRODUCTION

Bi is the heaviest stable element. Although the nearest-neighbor coordination number of approximately 10 is as large as that of simple liquid metals, the structure factor $S(Q)$ of liquid Bi, where Q is momentum transfer, exhibits a shoulder at the high momentum transfer side of the first maximum [1–3], in contrast to a symmetrical profile of simple liquid metals (see Fig. 1). Hence, liquid Bi is classified as a nonsimple liquid metal, as solid Bi is not a metal but a semimetal. The origin of the shoulder in $S(Q)$ of liquid Bi was theoretically studied and it was found that a model potential with a ridge in the repulsive component could reproduce the shoulder [4,5].

Bi belongs to the same group as As in the periodic table, and the local structure of liquid Bi has been discussed from a viewpoint of the Peierls distortion. The Peierls distortion is realized in crystalline As or Bi, whose structures are comprised of three short and three long bonds in a distorted simple cubic structure to minimize the energy. Such anisotropic bonding was observed in liquid As [6], and Peierls distortion has been investigated in liquid systems [7,8]. An *ab initio* molecular dynamics (AIMD) simulation for liquid Bi [9] suggested that longer and shorter bonds produce a distinct shoulder at the first peak in $S(Q)$.

The atomic dynamics of liquid Bi was studied by inelastic neutron scattering (INS) experiments in the 1980s. Dahlborg and Olsson [10,11] reported no distinct excitation of the acoustic mode in the dynamic structure factor $S(Q,E)$ at $Q > 6$ nm^{-1}, where E is energy transfer. Later, Dzugutov and Dahlborg [4] also found no distinct excitation of the acoustic mode at $Q > 6$ nm^{-1} with a classical molecular dynamics simulation, and concluded that this was the result of the unusual pair potential of liquid Bi. Meanwhile, in 1984, Shibata *et al.* [12] reported experimental observation of the acoustic mode up to 12 nm^{-1}.

Studies of atomic dynamics in liquid Bi have been revisited more recently. An INS experiment published in 2007 [13] confirmed that the inelastic excitations arising from the acoustic mode exist only at $Q \leqslant 6\,nm^{-1}$. In contrast, an *ab initio* molecular dynamics (AIMD) simulation by Souto *et al.* [9] reported that the inelastic excitation of the acoustic mode survives up to 14 nm^{-1}. Furthermore, the AIMD simulation predicted anomalous dispersion of the acoustic mode in liquid Bi with the excitation energy almost constant from 8 to 17 nm^{-1}. This behavior is much different from that in simple liquid metals, where the acoustic mode energy usually exhibits a maximum approximately at Q half of the first peak position of $S(Q)$ [14].

As described above, the previous INS measurements of liquid Bi show inconsistency for the inelastic excitation of the acoustic mode, and these results are also different from the AIMD prediction that indicates peculiar atomic dynamics arising from an anisotropic interatomic force in this monatomic liquid. Hence, it is important to observe the inelastic excitation of the acoustic mode in liquid Bi using inelastic x-ray scattering (IXS) because the IXS technique allows us to avoid the kinematic constraints of neutron scattering and obtain good spectra out to large energy transfers. The very high photoelectric x-ray absorption of Bi makes IXS experiments somewhat difficult, however, with modern facilities, they are possible.

We carried out IXS experiments to obtain $S(Q,E)$ of liquid Bi and determined the dispersion curve of the excitation energy of the acoustic mode experimentally. Our IXS data then show clear excitations in $S(Q,E)$ out to at least 12 nm^{-1}. Further, and consistent with the AIMD simulations of [9], we find a flat region of the acoustic dispersion curve. We compare our IXS results with the previous INS measurements, and by comparing the spectra, arrive at a reasonably consistent picture of the various data sets. We also present new *ab initio* and classical MD simulations, which are compared with experiment, and with previous calculations. Finally, we discuss our results in the context of previous work [15–20] and suggest a possible mechanism for the unusual dispersion of liquid Bi.

II. EXPERIMENTAL PROCEDURE AND COMPUTER SIMULATION

The experiments were conducted at the high-resolution IXS beamline (BL35XU) of SPring-8 in Japan [21]. Backscattering

*masinui@hiroshima-u.ac.jp

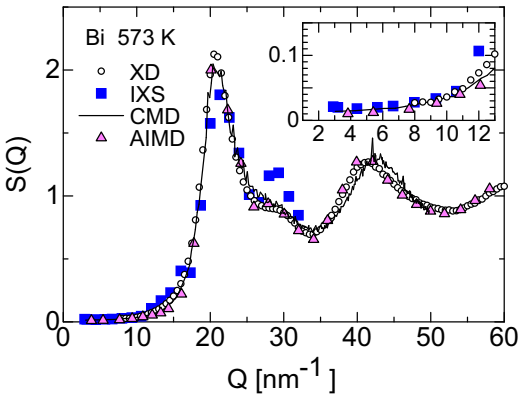

FIG. 1. (Color online) $S(Q)$ of liquid Bi at 573 K. Open dots and blue squares denote the result obtained by our own x-ray diffraction experiments at BL04B2/SPring-8 and the integration of IXS data, respectively. Also shown are our CMD (solid line) and AIMD (pink triangles) results. The inset shows $S(Q)$ at $Q \leqslant 13$ nm^{-1} on an enlarged scale.

at the Si (11 11 11) reflection provided a beam of approximately 10^{10} photons/s in an 0.8-meV bandwidth onto the sample. The energy of the incident beam and the Bragg angle of the backscattering were 21.747 keV and approximately 89.98°, respectively. We used 12 spherical analyzer crystals at the end of the 10-m horizontal arm. The spectrometer resolution was approximately 1.5 meV depending on the analyzer crystal, as measured using scattering from polymethyl methacrylate (PMMA). The Q resolution ΔQ was set to be 0.45 and 1.0 nm^{-1} (full width) for $Q \leqslant 11$ and $Q > 11$ nm^{-1}, respectively.

Liquid Bi of 99.999% purity was mounted in a single-crystal sapphire cell of Tamura-type [22] that was carefully machined to provide a 0.04-mm sample thickness. The cell was placed in "Marburg" chamber [23]. IXS spectra were measured at 573 and 1023 K in pure He atmosphere at 0.1 MPa, and here we focus on the results at 573 K. Several thermodynamic quantities of Bi at 573 K are tabulated in Table I. Scans over a range from −30 to 30 meV required 2.5 h each and we carried out 12 scans at $2 < Q \leqslant 6$ nm^{-1} (∼30 h of data collection), 8 scans at $6 < Q \leqslant 11$ nm^{-1}, and 4 scans at $11 < Q \leqslant 17$ nm^{-1} and 2 scans at $17 < Q \leqslant 32$ nm^{-1} to obtain good quality spectra. Background spectra were measured at 573 K with an empty cell. After scaling for sample transmission, the backgrounds were subtracted from the data, and $S(Q,E)/S(Q)$ were obtained. The weak peak in the 2.9-nm^{-1} spectrum at approximately 13 meV is consistent with the transverse acoustic (TA) mode energy of sapphire and is due to incomplete background subtraction: the cell position was slightly off center during the sample measurement and it is probable that the x-ray beam grazed the side of the sapphire cell.

TABLE I. The specific-heat ratio γ [14], mass density ρ [35], thermal conductivity Λ [35], heat capacity at the constant pressure C_p [35], and adiabatic sound velocity $c_{\rm ad}$ [36] of liquid Bi at temperature T. The melting point of Bi is 544 K.

T (K)	γ	ρ (g/cm^3)	Λ [W/(m K)]	C_p [J/(g K)]	$c_{\rm ad}$ (m/s)
573	1.15	10.0	15.5	0.143	1624

Figure 1 shows $S(Q)$ at 573 K. $S(Q)$ was measured on a two-axis diffractometer with a high-temperature furnace installed at BL04B2/SPring-8. Monochromatized high-energy x rays of 113 keV were incident on the sample in a glass capillary of 0.3 mm in inner diameter, and scattered x rays were detected by a Ge detector. The details of the beamline and the deduction of structure factor $S(Q)$ from the raw diffraction data are described in Ref. [24]. We plot the energy integration of $S(Q,E)$ in Fig. 1. Note that the integration of the IXS $S(Q,E)$ was adjusted to $S(Q)$ of approximately 0.03 at 8 nm^{-1}. The integration of $S(Q,E)$ agrees fairly well with $S(Q)$ obtained by x-ray diffraction up to the vicinity of the $S(Q)$ maximum.

AIMD simulations were performed using the QUANTUM ESPRESSO package [25], which is based on the density functional theory, plane waves, and pseudopotentials. The generalized gradient approximation (GGA) [26] was adopted for the exchange-correlation energy. We used the norm-conserving pseudopotential Bi.pbe-hgh.UPF [27] for the electron-ion interaction with five valence electrons, $6s^2 6p^3$. The plane-wave cutoff energy for the electronic wave functions was 15 Ry. The Γ point was only used to sample the Brillouin zone of the MD supercell. We used 128 Bi atoms in a cubic MD cell with periodic boundary conditions. The length of the side of the MD cell was 1.6422 nm. The MD simulation was performed on the ground-state Born-Oppenheimer surface at 573 K for 32 000 steps with a time step of 4.8 fs. Dynamic properties were calculated by averaging over atomic configurations of 30 000 steps after the thermodynamic equilibrium was established. More details may be found in [28]. $S(Q)$ obtained by our AIMD simulation agrees with that obtained by x-ray diffraction as shown in Fig. 1. The integration of the IXS $S(Q,E)$ agrees with the AIMD $S(Q)$ at $Q < 11$ nm^{-1} but the IXS $S(Q,E)$ becomes larger at $12 \leqslant Q \leqslant 16$ nm^{-1}.

We also carried out a classical MD (CMD) simulation at 573 K using the model potential reported in [4] for a system with 256 particles, and confirmed that $S(Q)$ of liquid Bi is well reproduced as shown in Fig. 1. To obtain $S(Q,E)$, the simulation was performed at 573 K for 60 000 steps with a time step of 2.4 fs. As reported previously [4], no clear inelastic excitations were visible in the spectra for $Q > 6$ nm^{-1}: the classical MD simulations reproduce $S(Q)$ but fail for $S(Q,E)$.

III. RESULTS

Figure 2 shows $S(Q,E)/S(Q)$ of liquid Bi observed at 573 K. The profile at low Q exhibits a central peak with the acoustic mode clearly visible on each side. The mode disperses with increasing Q, and $S(Q,E)/S(Q)$ exhibits a prominent excitation approximately at ±8 meV at $Q \geqslant 6$ nm^{-1}. At 14.6 nm^{-1}, the acoustic excitation is broad but still clearly visible. Blue curves in Fig. 2 denote $S(Q,E)/S(Q)$ obtained by our AIMD simulation. In order to compare them with the IXS results, the AIMD $S(Q,E)$ were obtained by a window corresponding to the experimental resolution, and the AIMD $S(Q,E)/S(Q)$ at similar Q values were corrected with the

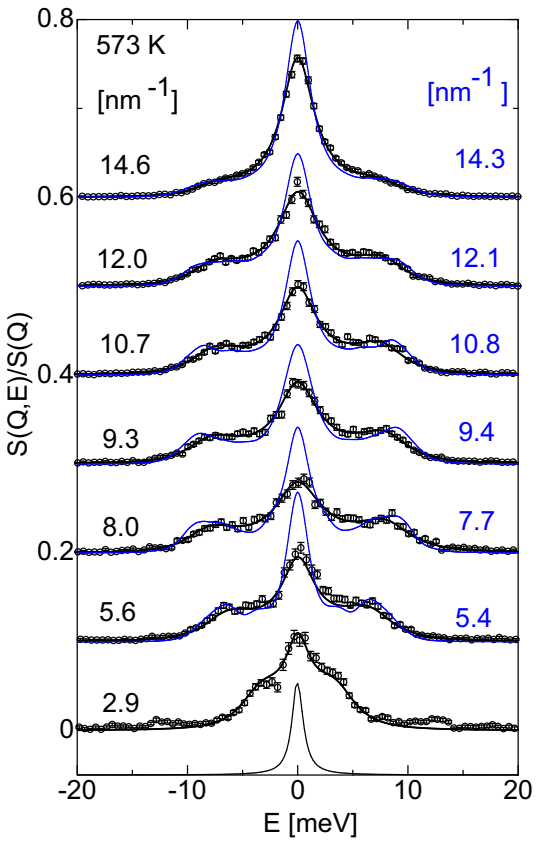

FIG. 2. (Color online) $S(Q,E)/S(Q)$ of liquid Bi at 573 K. Q values are indicated at the left side in the frame. Open circles and bold solid lines denote experimental results and the fits using the memory function formalism, respectively. Thin solid curves at the bottom denote the resolution function. Also shown is $S(Q,E)/S(Q)$ obtained by our AIMD simulation (blue curves). Q values of the AIMD curves are indicated at the right side. The IXS data at 2.9 nm^{-1} exhibit a peak at ± 13 meV, due to incomplete background subtraction (see Sec. II).

detailed balance factor. The quasielastic component of the AIMD results is systematically higher than the measured one while the energy integration of AIMD $S(Q,E)$ agrees with that of the IXS data at low Q, as shown in Fig. 1. A higher quasielastic peak in the AIMD results was also reported by Souto *et al.* [9] where the results were compared with INS [13]. They also obtained the self-diffusion coefficient that agrees with the lowest experimental data of liquid Bi. These results hint strongly that the higher quasielastic peak of the AIMD results in liquid Bi may be related to the well-known fact that the diffusion coefficient calculated in simulations of small systems becomes small [29,30]. The inelastic peak position in the AIMD $S(Q,E)$ is located at slightly higher energy than that of the IXS, as the shift of the peak position is evidently observed at $7 < Q < 11$ nm^{-1}.

Figure 3 shows the experimental spectra normalized by their integral and scaled to the x-ray diffraction data at $Q = 8$ nm^{-1}. It includes the measured results from Dahlborg and Olsson [10,11], Sani *et al.* [13], and Shibata *et al.* [12]. Although the energy resolution and energy maximum of each spectrum is different, the profile of each spectrum qualitatively agrees with each other. The inelastic component of the INS data seems to disperse from 4 meV at 3 nm^{-1} to 7 meV at 11 nm^{-1}. The damping of the collective mode in each $S(Q,E)$ is approximately similar. However, $S(Q,E)$ of the INS at $Q \leqslant 11$ nm^{-1} is truncated at the energy where the inelastic excitation exists, possibly due to kinematic constraints of INS. This might have led Dahlborg and Olsson to conclude that no collective excitation of the acoustic mode exists for $Q > 6$ nm^{-1}. In fact, Dahlborg and Olsson actually found an inelastic excitation in $S(Q,E)$ at higher momentum transfers, 13 and 15 nm^{-1} (where INS kinematic constraints are less severe), and attributed it to multiple scattering effects because of intensity limits of the data. In contrast, the IXS, without kinematic constraints, and with no multiple scattering, allows clear spectra to be collected over a large energy range at all momentum transfers, making it easier to identify the collective modes.

We analyzed the IXS data using the memory function formalism for a simple liquid. Although liquid Bi is expected to have an anisotropic local structure, we assumed that the formalism can be applied to the experimentally obtained $S(Q,E)$ that is directionally averaged. The second-order memory function recently utilized for classical fluids is represented by the fast (μ) and slow (α) viscous decay and thermal (th) decay channels [31–34] as

$$M_2(Q,t) = 2\Gamma_\mu\,\delta(t) + \left[\omega_\ell^2(Q) - \gamma\omega_0^2(Q)\right]\exp[-t/\tau_\alpha(Q)] + (\gamma - 1)\omega_0^2(Q)\exp(-D_{\rm th}Q^2 t), \quad (1)$$

where γ, $\omega_0(Q)$, $\omega_\ell(Q)$, τ_α, and $D_{\rm th}$ are, respectively, the specific-heat ratio, the normalized second and fourth frequency moments, the relaxation time of α process, and the thermal diffusivity $D_{\rm th} = \Lambda/(\rho C_p)$, where Λ, ρ, and C_p are the thermal conductivity, the mass density, and the heat capacity at the constant pressure. The second frequency moment sum rule provides the relation $\omega_0^2(Q) = k_{\rm B}TQ^2/[mS(Q)]$, where m is atomic mass.

We took γ, ρ, Λ, and C_p, as shown Table I, as determined by thermodynamic measurements. The model function obtained by $\tilde{M}_2(Q,iE)$, the Fourier-Laplace transform of $M_2(Q,t)$, is given by

$$\left[\frac{S(Q,E)}{S(Q)}\right]^{\rm m} = \frac{1}{\pi}Re\left[\frac{iE + \tilde{M}_2(Q,iE)}{\omega_0^2(Q) - E^2 + iE\tilde{M}_2(Q,iE)}\right]. \quad (2)$$

To fit the model function with $S(Q,E)/S(Q)$ experimentally obtained, the function was convoluted with the detailed balance condition $B(E) = (E/k_BT)/\{1 - \exp(-E/k_BT)\}$ and the resolution function $R(E)$ as

$$\frac{S(Q,E)}{S(Q)} = \int dE' B(E')\,y(Q)\left[\frac{S(Q,E')}{S(Q)}\right]^{\rm m} R(E - E'). \quad (3)$$

Γ_μ, $\omega_0(Q)$, $\omega_\ell(Q)$, and $\tau_\alpha(Q)$ were optimized to fit $S(Q,E)/S(Q)$ obtained by IXS, and $y(Q)$ adjusting the amplitude of $S(Q,E)/S(Q)$ was optimized approximately at unity.

As shown in Fig. 2 (see also Fig. 6), the optimized model function reproduced the experimental data nicely. The χ^2 per degrees of freedom is reasonably distributed from 1.2 to 1.8 at $Q \leqslant 15$ nm^{-1} but it exceeds 2.0 at higher Q. This is mostly

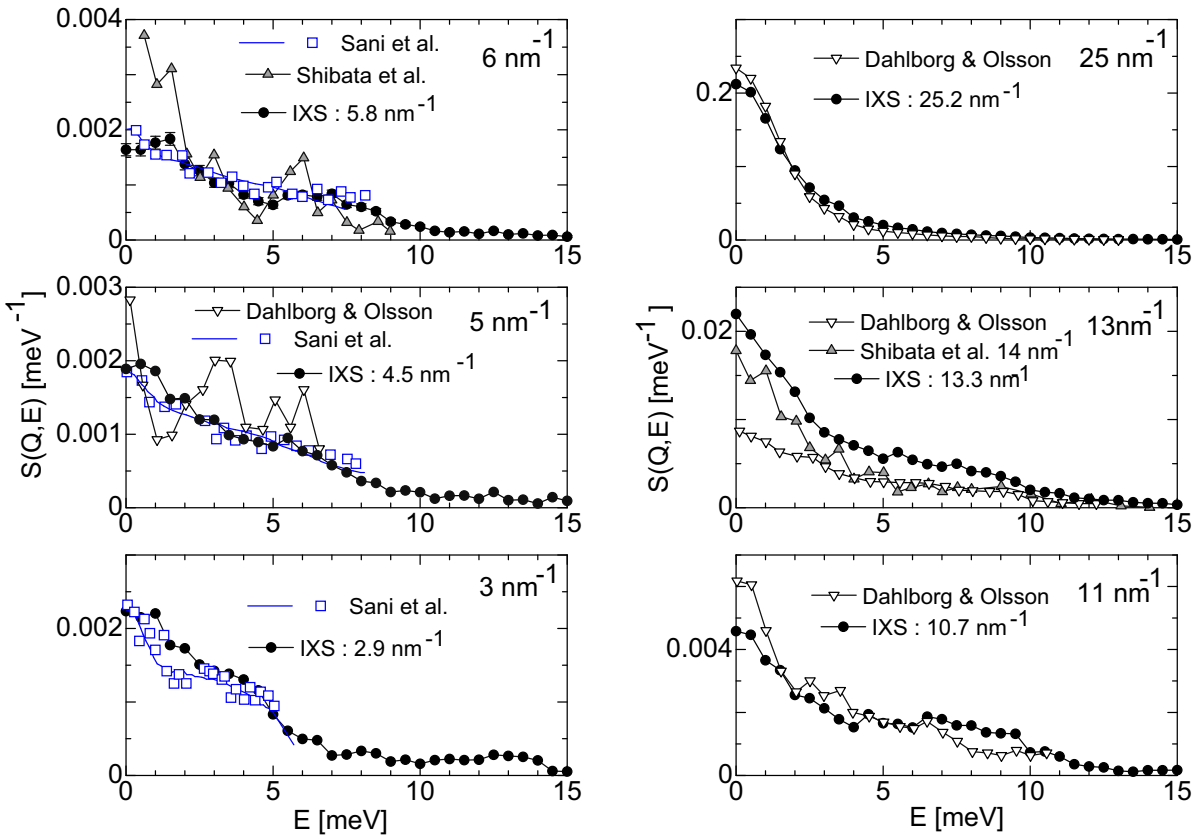

FIG. 3. (Color online) Comparison of the present IXS results to previous INS work. Blue open squares (experimental data) and a blue line (fits) denote $S(Q,E)$ at 580 K reported by Sani *et al.* [13], and upside-down triangles denote those by Dahlborg and Olsson [10,11]. $S(Q,E)$ at 673 K by Shibata *et al.* [12] is denoted by gray triangles. Q values of these INS results are indicated at the right side in the frame.

because the statistical errors in $S(Q,E)/S(Q)$ became small at higher Q near the $S(Q)$ maximum and so the fits become sensitive to small deviations in the model.

The excitation energy of the acoustic mode $\omega_{\rm p}(Q)$ was defined as a peak position of the current-current correlation function $C(Q,E) = E^2[S(Q,E)]^{\rm m}/Q^2$, where $[S(Q,E)]^{\rm m}$ is the model function before convolution. Figure 4 shows $\omega_0(Q)$, $\omega_{\rm p}(Q)$, and $\omega_\ell(Q)$ of liquid Bi at 573 K. $\omega_{\rm p}(Q)$ linearly disperses up to 7 nm^{-1} along approximately 2170 m/s, which is 34% faster than the adiabatic sound speed $c_{\rm ad}$. $\omega_{\rm p}(Q)$ at $2.9 \leqslant Q \leqslant 6$ nm^{-1} is consistent with the previous INS result reported by Sani *et al* [13]. $\omega_{\rm p}(Q)$ deviates from the linear dispersion and stays at approximately constant at 8.5 meV at $10 \leqslant Q \leqslant 15$ nm^{-1}. A flat region in the dispersion curve is consistent with the prediction by the AIMD simulation [9] although the AIMD results lie at slightly higher energy as shown in Fig. 4. Our IXS results then qualitatively confirm the theoretical prediction. A dashed-dotted line in Fig. 4 shows $\omega_{\rm p}(Q)$ obtained by our CMD. The dashed-dotted line at low Q seems to be connected to the line of $c_{\rm ad}$, but black circles is located at higher energy than the dashed-dotted line at $Q < 10$ nm^{-1}. The result suggests that the pair potential providing a good fit to $S(Q)$ does not properly reproduce the long-range interatomic interaction in liquid Bi.

For IXS results, the optimized $\omega_\ell(Q)$ is slightly smaller than $\omega_{\rm p}(Q)$ at $Q < 6$ nm^{-1} although the memory function formalism requires $\omega_\ell(Q) \geqslant \omega_{\rm p}(Q)$. The result may imply that

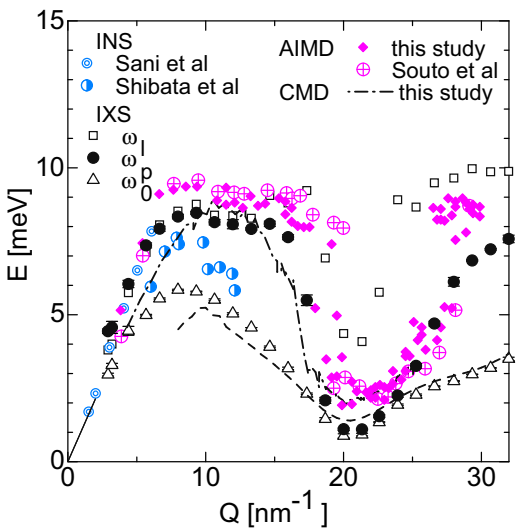

FIG. 4. (Color online) $\omega_\ell(Q)$ (open squares), $\omega_{\rm p}(Q)$ (black circles), and $\omega_0(Q)$ (open triangles) obtained by IXS results at 573 K. $\omega_{\rm p}(Q)$ by AIMD simulations of this study and that at 600 K [9] is indicated by diamonds and circles with cross, respectively. Also shown are the excitation energy obtained by INS by Sani *et al.* (double circles) and by Shibata *et al.* (circles with half moon), and CMD (dashed-dotted line). The ultrasonic sound speed is denoted by a black line. A broken line denotes $\omega_0(Q)$ calculated by the sum rule with experimentally obtained $S(Q)$ shown in Fig. 1.

$\omega_p(Q)$ obtained from $C(Q,E)$ at $Q < 6$ nm^{-1} overestimates the real excitation energy [$\approx \omega_\ell(Q)$] due to the broadening of IXS data.

IV. DISCUSSION

In order to understand the dispersion observed in liquid Bi, it is useful to consider phonon dispersion in crystalline (c-)Bi where there is known to be a Peierls distortion. Yarnell *et al.* [37] carried out INS on c-Bi and reported the dispersion curves of the longitudinal and transverse acoustic modes (LA and TA, respectively) and the optical modes (LO and TO) along the trigonal and binary directions. They analyzed these phonon dispersion curves using a linear chain model with two atoms per unit cell. In the model, they took account of the interaction of atoms up to the second-neighbor unit cells and used six force constants to obtain dispersion curves consistent with the experimental results.

We plot the branches reported by Yarnell *et al.* [37] in Fig. 5. $\omega_p(Q)$ of liquid Bi disperses along the LA dispersion curves at low Q. The result suggests a possibility that the atomic dynamics in liquid Bi can be analyzed using a crystal-like approach that was recently applied to the high-frequency dynamics of liquid Ga at normal [15] and high pressures [17], and liquid Na at high pressure [16]. In that work, the broad quasielastic contribution in $S(Q,E)$ in the liquids was explained by pure quasielastic and quasitransverse acoustic components, and these liquids at high pressures show that a quasitransverse component disperses similarly to the TA branch of the corresponding crystals at low Q.

Considering the previous studies of a crystalline Bi, we fit $S(Q,E)/S(Q)$ of liquid Bi using a model function composed of a single Lorentzian and two damped harmonic oscillators (DHO) [39]. For comparison, we also carried out the fits using a single Lorentzian and a single DHO. To obtain the optimized parameters, $y(Q)\,[\frac{S(Q,E')}{S(Q)}]^m$ in Eq. (3) was replaced with these model functions.

Figure 6 shows the optimized curve of each model function and the residuals. The single DHO model could not reproduce $S(Q,E)/S(Q)$ reasonably for $Q > 6$ nm^{-1} and the dual DHO model was surely needed. In fact, by carrying out Bayesian analysis [40], we confirmed that the dual DHO model is validated at 6.6 and 12.0 nm^{-1} while the single DHO model at 4.3 nm^{-1}. (At $Q = 4.3$ nm^{-1}, the single and dual DHO models give essentially identical fits, with the second DHO amplitude negligibly small: the reduced χ^2 per a degree of freedom for the single DHO fit comes from the reduction in number of fit parameters.) As plotted in Fig. 5, the excitation energy of the acoustic mode in the single DHO model ($\omega - 1$DHO) agrees with $\omega_p(Q)$ fairly well at low Q but it shifts to lower energy at $Q > 8$ nm^{-1}. At $7 < Q < 15$ nm^{-1}, the higher excitation energy $\omega_1 - 2$DHO of the dual DHO model shows an approximately flat dispersion similarly to black circles.

The lower excitation energy of the dual DHO model $\omega_2 - 2$DHO lies at approximately 5 meV near the trigonal zone boundary. Upon shifting to higher energy at 8 nm^{-1}, it decreases with further increasing Q. Meanwhile, the previous AIMD [9] predicted that the transverse acoustic mode in liquid Bi becomes bimodal for $Q \geqslant 9$ nm^{-1} and the lower excitation energy disperses approximately at 2 meV as shown in Fig. 5.

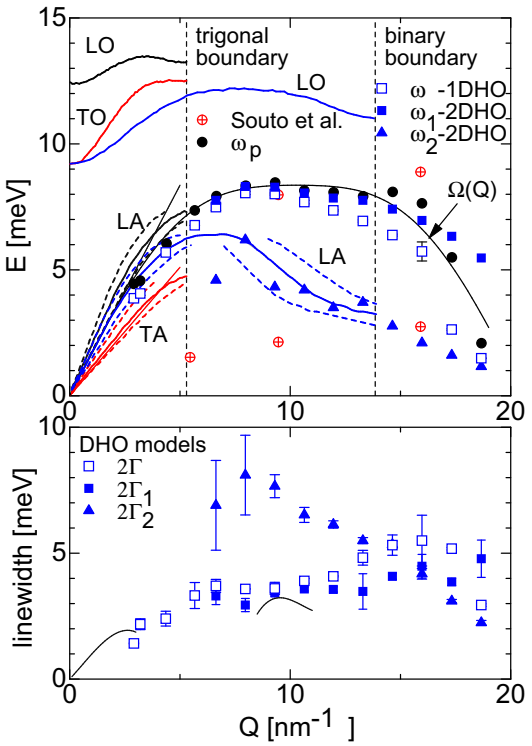

FIG. 5. (Color online) Comparison to measurements of crystalline Bi. Bold black and red lines denote dispersion curves of the longitudinal acoustic (LA) and transverse acoustic (TA), and longitudinal optical (LO) and transverse optical (TO) modes along the trigonal direction. LA and LO modes along the binary direction are denoted by bold blue lines. Broken lines on both side of the LA and TA modes represent the smearing of the Brillouin zone due to the disorder estimated from the FWHM of the first peak of $S(Q)$ [17]. Black circles denote $\omega_p(Q)$ obtained by the memory function analysis. The excitation energies obtained by the single DHO model (blue open squares), and those by the dual DHO model (solid blue symbols) are shown. The peak energy of the transverse $C(E,Q)$ reported by Souto *et al.* at 600 K [9] is denoted by circles with cross. The dispersion lines of longitudinal and transverse sound speeds [38] are denoted by black and red lines at $0 \leqslant Q \leqslant 5$ nm^{-1}, respectively. The optimized dispersion curve $\Omega(Q)$ is denoted by a thin black curve. The lower panel shows the linewidth of the excitation energies from DHO models. Black lines at $Q \leqslant 3$ nm^{-1} and at $8.5 \leqslant Q \leqslant 11$ nm^{-1} denote FWHM estimated from the solid data, using the same disorder as mentioned above [17].

The bimodal nature of the transverse acoustic mode was confirmed by our AIMD. Although the discrepancy between $\omega_2 - 2$DHO and the AIMD transverse acoustic excitation energy is not neglected at low Q, the discrepancy becomes small at higher Q. Hence, it will be possible to assign $\omega_2 - 2$DHO as the excitation energy of a quasitransverse acoustic component. It is also possible to carry out the analysis assuming the two DHO modes are coupled, as discussed in [18], and in that case we find reasonable fits can be obtained, but the values of U are not well determined.

Alternatively, Bryk and Mryglod [19,20] reported the excitation energy that shows Q dependence similar to $\omega_2 - 2$DHO. They investigated collective excitations in liquid Bi within the nine variable approximations of the generalized collective

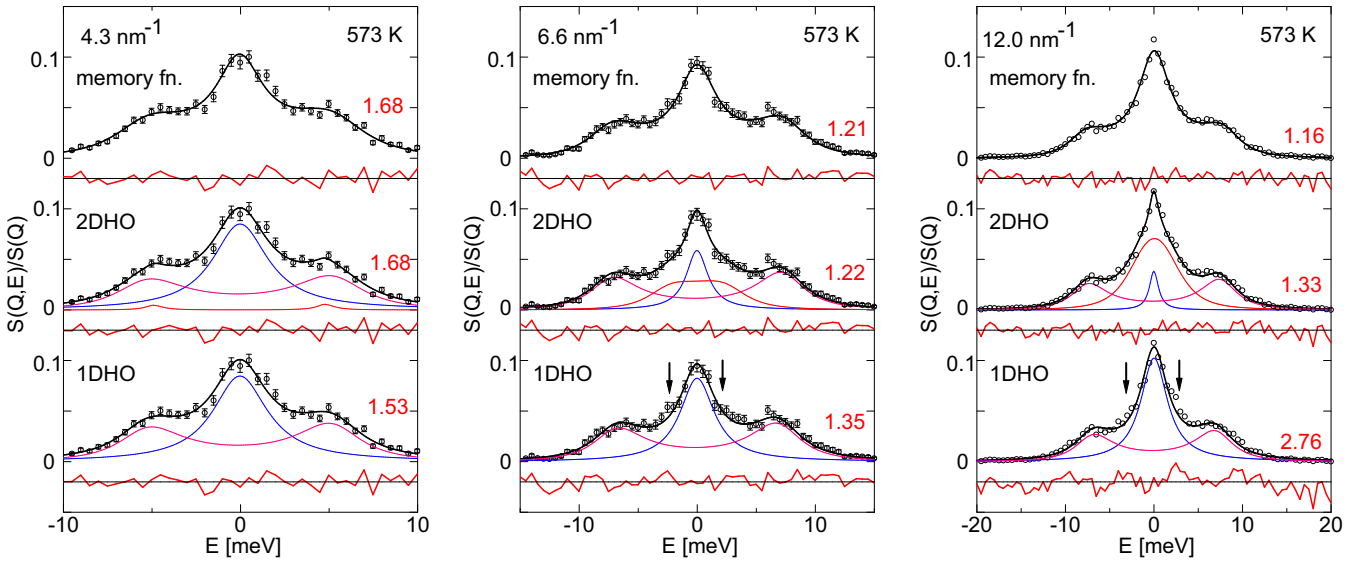

FIG. 6. (Color online) $S(Q,E)/S(Q)$ of liquid Bi at Q indicated in each panel. Circles denote IXS results and solid curves indicate the best fits using memory function analysis, the single DHO (1DHO) and dual DHO (2DHO) models, as indicated. The quasielastic (blue) and inelastic (magenta and red) components of the DHO model functions are denoted by thin lines. The residuals properly scaled are plotted below each spectrum. The χ^2 per a degree of freedom for each result is indicated by a red number. At $Q \geqslant 6.6$ nm^{-1}, the residuals in the vicinity of Q indicated by arrows are reduced by a 2DHO model.

mode (GCM) approach with their CMD simulation. The GCM analysis provided the excitation energy of the acoustic mode as the imaginary part of a complex eigenvalue $\mathrm{Im}(z_1^{\pm})$. The analysis predicted the other three relaxing collective modes with purely real eigenvalues. Among them, the energy of the kinetic mode d_2 decreases with increasing Q similarly to $\omega_2 - 2\mathrm{DHO}$ at $Q > 7$ nm^{-1}. However, as the profile of the kinetic mode is theoretically modeled by a Lorentzian, we think that a possibility is small that $\omega_2 - 2\mathrm{DHO}$ corresponds to d_2.

The lower panel of Fig. 5 shows the linewidth (2Γ, see Ref. [39]) of the collective modes obtained by fitting with a DHO model. We used a single DHO for $Q \leqslant 6$ nm^{-1} and a dual DHO model for higher Q (see Fig. 6 and discussion). These are compared with an expected linewidth estimated from the dispersion of the LA and TA modes of the solid, as discussed in [17]. There, momentum blurring consistent with the width of the $S(Q)$ maximum of the liquid is assumed to broaden the modes at very low Q. Here, we find reasonable agreement with the model of [17] for the longitudinal excitations, but not the transverse excitations. However, we are also at much higher Q than [17] so the simple model of broadening suggested there may not be sufficient.

Here, we mention the relationship between the memory function analysis and the present crystal-like approach. The model function of $S(Q,E)/S(Q)$ deduced from Eq. (1) is expressed by a rational function whose denominator is a polynomial of degree 4. Using the optimized parameters, we found that the solution of the polynomial is composed of two real and one complex conjugate values except for the vicinity of the $S(Q)$ maximum. The result means that the model function deduced from the memory function is equivalent to that with two Lorentzian and one DHO functions. Hence, as shown in Fig. 6, the optimization with the memory function analysis is better than that with 1DHO model at $Q > 6$ nm^{-1}.

As shown in Fig. 5, there is a wide-Q region between the zone boundaries along the trigonal and binary directions in c-Bi, and a flat region of the dispersion curve of $\omega_{\mathrm{p}}(Q)$ appears between these zone boundaries where LA and LO branches along the binary direction disperse. This fact hints that an interaction between the LA and LO branches may be related to the dispersion curve of $\omega_{\mathrm{p}}(Q)$ flat in the liquid state. Here, we consider a one-dimensional model to represent such an interaction. When a lattice wave of a simple linear chain model is considered, the phonon energy $\Omega(Q)$ with the Peierls distortion may be modeled by

$$\Omega(Q)^2 = \Omega_1^2[1 - \cos(Qa)] + \Omega_2^2[1 - \cos(2Qa)], \qquad (4)$$

where a, Ω_1, and Ω_2 are a lattice constant, eigenfrequencies determined by first- and second-nearest-neighbor force constants, respectively. Another interpretation of the force constants is that Ω_1 and Ω_2 are the intradimer and interdimer interactions in the Peierls distortion, respectively. This interpretation may be consistent with that the optical mode in the unit cell with two atoms is taken into account. Interestingly, Eq. (4) gives a flat dispersion curve when the ratio of Ω_2/Ω_1 is fixed to be 0.5. As shown in Fig. 5, when $\omega_{\mathrm{p}}(Q)$ obtained by IXS is fitted up to 19 nm^{-1} using Eq. (4), Ω_1, Ω_2, and a are optimized to be 8.98 ps^{-1}, 4.14 ps^{-1}, and 0.306 nm, respectively. The optimized a is slightly shorter than the first peak position of the pair distribution function, corresponding to a shorter bond in liquid Bi [9]. The first component of Eq. (4) gives the sinusoidal outline of the dispersion curve, and the curve is flattened by the second component arising from a medium-range correlation at $2a$ of approximately 0.6 nm. This result is consistent with the fact that the long-range interatomic interaction is needed to reproduce the dispersion curve at low Q as suggested by our CMD results.

The results of our simple linear chain model should catch an essential mechanism of the flat dispersion in liquid Bi when

a pseudo-Brillouin zone concept in a disordered system is applied [41], and they may be considered as experimental evidence of the Peierls distortion realized in liquid Bi. A possible scenario of the Peierls distortion in liquid Bi is that the layer structure composed of threefold-coordinated atoms in c-Bi is preserved as layered clusters on melting. Then, the force constant of strong bonds in the cluster gives Ω_1 while that of weak bonds between clusters gives Ω_2. The average distance between adjacent clusters is estimated approximately twice as large as the intracluster bond distance by considering a pairing of atoms in a simple cubic structure [8]. From these considerations, we suggest that the cooperation of short- and medium-range interatomic interactions with different force constants is a possible mechanism of the flat region of the dispersion curve of the acoustic mode observed in liquid Bi.

V. SUMMARY

IXS experiments for liquid Bi clearly show a distinct inelastic excitation of the acoustic mode observable in $S(Q,E)$ at $Q > 6$ nm^{-1}, resolving previous disagreement in the literature [4,9–13]. The excitation energy of the acoustic mode obtained by the memory function analysis for the IXS data behaves similarly to the AIMD simulation [9] and in particular, has a flat, dispersionless behavior between 7 and 15 nm^{-1}. The dispersionless behavior is also confirmed by an alternative analysis of the data using a dual DHO + Lorentzian model.

When a crystal-like approach with the model function composed of a Lorentzian and two DHO functions is applied to the IXS data of liquid Bi, the higher excitation energy of the DHO component, corresponding to the longitudinal acoustic mode, disperses similarly to that obtained by the AIMD. The lower-energy DHO component seems consistent with that of the quasitransverse acoustic excitation at low Q.

Based on the results obtained by the AIMD and CMD simulations, and our one-dimensional model for the IXS data, we suggest that the peculiar dispersion of the acoustic mode observed in liquid Bi may be related to the Peierls distortion in the crystalline state, where long-range interatomic interaction plays an important role. Our model also suggests a possibility that the flat region of the dispersion curve is related to the optical mode.

ACKNOWLEDGMENTS

The authors would like to acknowledge Dr. S. Kohara and Dr. W.-C Pilgrim for their valuable discussion, and would like to thank the Ministry of Education, Culture, Sports, Science and Technology, Japan, for a Grant-in-Aid for Scientific Research. The synchrotron radiation experiments were performed at the SPring-8 with the approval of the Japan Synchrotron Radiation Research Institute (JASRI) (Proposals No. 2011B1314, No. 2010B1173, and No. 2009B1283).

[1] M. North, J. E. Enderby, and P. A. Egelstaff, J. Phys. C: Solid State Phys. **1**, 1075 (1968).
[2] Y. Waseda and K. Suzuki, Phys. Status Solidi B **49**, 339 (1972).
[3] Y. Greenberg, E. Yahel, E. N. Caspi, C. Benmore, B. Beuneu, M. P. Dariel, and G. Makov, Europhys. Lett. **86**, 36004 (2009).
[4] M. Dzugutov and U. Dahlborg, Phys. Rev. A **40**, 4103 (1989).
[5] J. Hafner and W. Jank, Phys. Rev. B **45**, 2739 (1992).
[6] R. Bellissent, C. Bergman, R. Ceolin, and J. P. Gaspard, Phys. Rev. Lett. **59**, 661 (1987).
[7] C. Bichara, A. Pellegatti, and J. P. Gaspard, Phys. Rev. B **47**, 5002 (1993).
[8] A. Chiba, M. Tomomasa, T. Hayakawa, S. M. Bennington, A. C. Hannon, and K. Tsuji, Phys. Rev. B **80**, 060201(R) (2009).
[9] J. Souto, M. M. G. Alemany, L. J. Gallego, L. E. González, and D. J. González, Phys. Rev. B **81**, 134201 (2010).
[10] U. Dahlborg and L. G. Olsson, Phys. Rev. A **25**, 2712 (1982).
[11] U. Dahlborg and L. G. Olsson, J. Phys. F: Met. Phys. **13**, 555 (1983).
[12] K. Shibata, S. Hoshino, and H. Fujishita, J. Phys. Soc. Jpn. **53**, 899 (1984).
[13] L. Sani, L. E. Bove, C. Petrillo, and F. Sacchetti, J. Non-Cryst. Solids **353**, 3139 (2007).
[14] T. Scopigno, G. Ruocco, and F. Sette, Rev. Mod. Phys. **77**, 881 (2005).
[15] S. Hosokawa, M. Inui, Y. Kajihara, K. Matsuda, T. Ichitsubo, W.-C. Pilgrim, H. Sinn, L. E. Gonzalez, D. J. Gonzalez, S. Tsutsui, and A. Q. R. Baron, Phy. Rev. Lett. **102**, 105502 (2009).
[16] V. M. Giordano and G. Monaco, Proc. Natl. Acad. Sci. USA **107**, 21985 (2010).
[17] V. M. Giordano and G. Monaco, Phys. Rev. B **84**, 052201 (2011).
[18] M. Zanatta, F. Sacchetti, E. Guarini, A. Orecchini, A. Paciaroni, L. Sani, and C. Petrillo, Phys. Rev. Lett. **114**, 187801 (2015).
[19] T. Bryk and I. Mryglod, J. Phys.: Condens. Matter **12**, 3543 (2000).
[20] T. Bryk and I. Mryglod, J. Phys.: Condens. Matter **13**, 1343 (2001).
[21] A. Q. R. Baron, Y. Tanaka, S. Goto, K. Takeshita, T. Matsushita, and T. Ishikawa, J. Phys. Chem. Solids **61**, 461 (2000).
[22] K. Tamura, M. Inui, and S. Hosokawa, Rev. Sci. Instrum. **70**, 144 (1999).
[23] S. Hosokawa and W.-C. Pilgrim, Rev. Sci. Instrum. **72**, 1721 (2001).
[24] S. Kohara, M. Itou, K. Suzuya, Y. Inamura, Y. Sakurai, Y. Ohishi, and M. Takata, J. Phys.: Condens. Matter **19**, 506101 (2007).
[25] P. Giannozzi, S. Baroni, N. Bonini, M. Calandra, R. Car, C. Cavazzoni, D. Ceresoli, G. L. Chiarotti, M. Cococcioni, I. Dabo, A. Dal Corso, S. Fabris, G. Fratesi, S. de Gironcoli, R. Gebauer, U. Gerstmann, C. Gougoussis, A. Kokalj, M. Lazzeri, L. Martin-Samos, N. Marzari, F. Mauri, R. Mazzarello, S. Paolini, A. Pasquarello, L. Paulatto, C. Sbraccia, S. Scandolo, G. Sclauzero, A. P. Seitsonen, A. Smogunov, P. Umari, and R. M. Wentzcovitch, J. Phys.: Condens. Matter **21**, 395502 (2009).
[26] J. P. Perdew, K. Burke, and M. Ernzerhof, Phys. Rev. Lett. **77**, 3865 (1996).
[27] http://www.quantum-espresso.org
[28] S. Munejiri, F. Shimojo, and K. Hoshino, Phys. Rev. B **86**, 104202 (2012).
[29] In-Chul Yeh and Gerhard Hummer, J. Phys. Chem. B **108**, 15873 (2004).

[30] S. Munejiri, T. Masaki, T. Itami, F. Shimojo, and K. Hoshino, Phys. Rev. B **77**, 014206 (2008).
[31] D. Levesque, L. Verlet, and J. Kürkijarvi, Phys. Rev. A **7**, 1690 (1973).
[32] U. Balucani and M. Zoppi, *Dynamics of Liquid State* (Clarendon, Oxford, 1994).
[33] T. Scopigno, U. Balucani, G. Ruocco, and F. Sette, J. Phys.: Condens. Matter **12**, 8009 (2000).
[34] F. Bencivenga, A. Cunsolo, M. Krisch, G. Monaco, G. Ruocco, and F. Sette, Phys. Rev. E **75**, 051202 (2007).
[35] *Metal Data Book*, edited by Y. Waseda (Maruzen, Tokyo, 2004).
[36] M. Inui, S. Takeda, and T. Uechi, J. Phys. Soc. Jpn. **61**, 3203 (1992).
[37] J. L. Yarnell, J. L. Warren, R. G. Wenzel, and S. K. Koenig, IBM J. Res. Dev. **8**, 234 (1964).
[38] Yakov Eckstein, A. W. Lawson, and Darrell H. Reneker, J. Appl. Phys. **31**, 1534 (1960).
[39] B. Fåk and B. Dorner, Physica B **234-236**, 1107 (1997).
[40] D. S. Sivia and J. Skilling, *Data Analysis, A Bayesian Tutorial*, 2nd ed. (Oxford University Press, Oxford, UK, 2006).
[41] T. Scopigno, M. D'astuto, M. Krisch, G. Ruocco, and F. Sette, Phys. Rev. B **64**, 012301 (2001).